International Journal of Energy and Environmental Engineering
a SpringerOpen Journal

ORIGINAL RESEARCH Open Access

CFD based analysis of flow distribution in a coaxial vacuum tube solar collector with laminar flow conditions

Abdul Waheed Badar*, Reiner Buchholz, Yongsheng Lou and Felix Ziegler

Abstract

A computational fluid dynamics (CFD) analysis has been conducted to find the pressure losses for dividing and combining fluid flow through a tee junction of a solar collector manifold. Simulations are performed for a range of flow ratios and Reynolds numbers, and equations are developed for pressure loss coefficients at junctions. A theoretical model based on successive approximations then is employed to estimate the isothermal and non-isothermal flow distribution in laminar range through a collector consisting of 60 vacuum tubes connected in parallel in a reverse (U-configuration) and parallel (Z-configuration) flow arrangement. The results are in reasonable agreement with the available experimental results for U-configuration. The proposed CFD based strategy can be used as a substitute to setting up and performing costly experiments for estimating junction losses.

Keywords: computational fluid dynamics, junction pressure loss coefficient, dividing manifold, combining manifold, flow distribution

Background

In a typical vacuum tube solar collector design, the fluid flow usually is divided in a manifold to risers connected in parallel. After extracting heat from the attached absorber, the fluid passages are combined in a manifold and the hot fluid is led to the user. Heat gain of a solar collector is affected by the flow rate through the individual risers, and uniform distribution is desirable to achieve the same thermal output from all the tubes for best performance, which is not the case in reality [1]. Both the collector's overall flow rate and flow nonuniformity affect the collector efficiency [2-4].

The risers are generally connected at right angles to the manifold, thus forming a tee joint at each connection which leads to local disturbances. A varying local pressure drop for a flow through such a manifold results in an uneven flow distribution through the whole collector. Wang and Yu [5] developed a numerical model to calculate the isothermal flow distribution using mass and momentum equations at each branch of the header system. Wang and Wu [6] proposed a discrete numerical model and demonstrated the flow and temperature distribution in a flat-plate solar collector for U- and Z-configurations by taking into account the effects of buoyancy and longitudinal heat conduction. Jones and Lior [7] developed a discrete hydrodynamic model, and the resulting nonlinear algebraic equations were solved numerically. For negligible buoyancy effects, they investigated the effects of geometrical parameters of the collector such as the ratio of riser to manifold diameter, number of risers, and length of risers on the flow nonuniformity. Fan et al. [4] carried out CFD calculations to estimate the flow and temperature distribution in a flat-plate solar collector consisting of 16 risers connected in U-configuration, having a tilt of 40°. The influences of flow rate, fluid properties, collector tilt, and collector inlet fluid temperature were investigated. Later, for the same collector, Fan and Furbo [8] studied the buoyancy effects on fluid and temperature distribution by means of CFD calculations. They found that at a certain low flow rate, buoyancy effects are of the same order as the pressure drop in the risers or even larger, which results in a more nonuniform flow distribution. The pattern of flow distribution reverses as compared to the case of high flow rate (25 l/min) with negligible buoyancy effects. Glembin

* Correspondence: awbdr@yahoo.com
Institut für Energietechnik, KT 2, FG Maschinen- und Energieanlagentechnik, Technische Universität Berlin, Marchstraße 18, Berlin 10587, Germany

et al. [2] experimentally investigated the flow distribution in a horizontally placed coaxial vacuum tube solar collector consisting of 60 parallel vacuum tubes connected in U-configuration. They adopted a procedure where flow distribution was calculated from the measured tube outlet temperatures for a range of inlet temperatures and mass flow rates.

An alternative way for the determination of flow distribution is to solve it as a piping network where flow is divided amongst the parallel piping, and each flow path leads to the same pressure loss. The riser components connected to the manifolds interrupt the smooth flow of the fluid in the manifolds and cause additional losses. One of the key parameters in evaluating the flow distribution through such a piping network is the pressure loss at the junctions of dividing and combining manifold. At the junctions, the pressure loss coefficient, in general, depends on the geometry of the component and the Reynolds number, just like the friction factor. However, when the Reynolds numbers are very large, it is usually assumed to be independent of the Reynolds number. Based on the experimental data for turbulent flow, these junction loss coefficients can be found in the literature in the form of analytical or empirical expressions characterized by branch angle, area ratio, and flow ratio [9,10], which are not appropriate to use for laminar flow conditions. On the other hand, Weitbrecht et al. [11] performed experiments on a collector with 10 risers connected in Z-configuration and used the experimentally obtained junction loss coefficients to determine the flow distribution analytically with laminar flow conditions, which form the basis for this paper.

The aim of this work is to demonstrate the alternate use of CFD simulations instead of experiments to estimate the pressure loss coefficients at the junctions for a range of locally changing flow ratios and Reynolds numbers, and using those to calculate the flow distribution theoretically. A theoretical approach as adopted by Weitbrecht et al. [11] is used to estimate the isothermal flow distribution in the horizontally placed collector for both U and Z-configurations. Temperature effects on fluid properties are also taken into account for non-isothermal flow distribution, but the buoyancy effects are neglected for a horizontally placed collector. Modeling results then are compared and validated with those predicted experimentally by Glembin et al. [2]. Moreover, the influence of various other parameters is also investigated.

Methods

Collector specification

The collector considered in this study consists of two modules having a total number of 60 vacuum tubes connected in parallel in U-configuration and placed horizontally as shown in Figure 1a. Each vacuum tube contains a flat absorber sheet of 0.1 m^2 area coated with

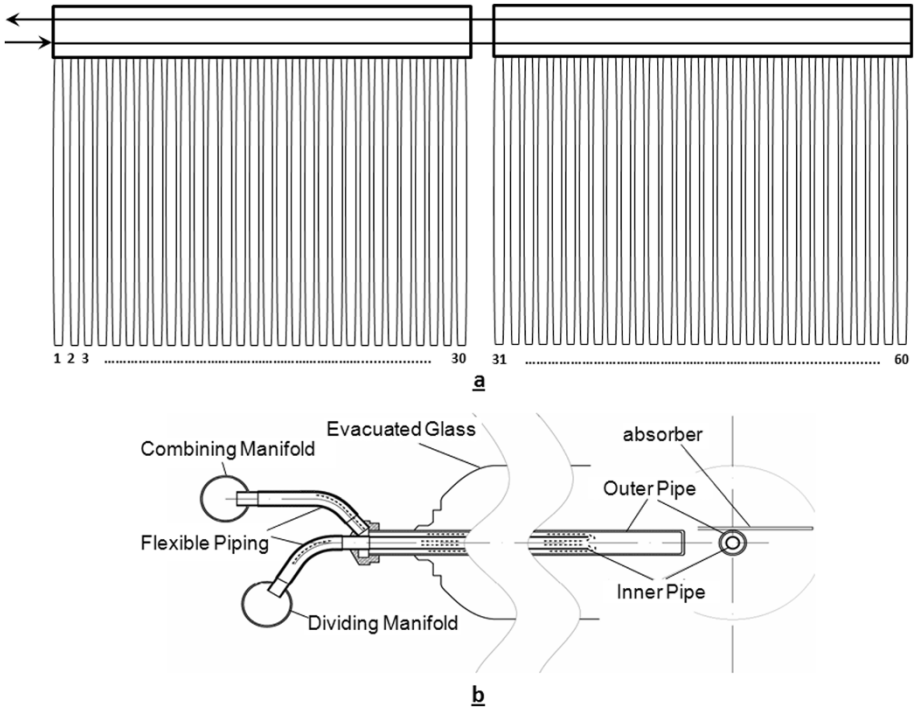

Figure 1 Schematic of the solar collector. (**a**) Collector group of 60 vacuum tubes (**b**) vacuum tube connected to manifold [12].

a selective surface (TiNOX) on a copper substrate and welded to the coaxial copper piping for fluid flow (Figure 1b [12]). A small part of the riser is intruded inside the manifolds, and flexible piping elements are used to connect the coaxial piping to the dividing and combining manifolds as illustrated in Figure 1b [12].

Table 1 summarizes the geometrical parameters of the collector. A mixture of water and propylene glycol [13] is used as a working fluid.

Junction pressure loss coefficients

The main focus of the study is to determine the pressure loss coefficients at the junctions. A part of the manifold attached to the riser forming a tee joint is taken into consideration for the analysis, and the actual flexible corrugated piping elements at inlet and outlet manifolds (Figure 1b) are assumed as straight pipe, as shown in Figure 2. The effect of adjacent branches on each other is not considered.

The loss coefficient k represents the energy dissipation at the junction and is defined as follows:

$$k = \frac{\Delta p}{\rho V_c^2/2}, \tag{1}$$

where Δp is the pressure drop between the upstream and downstream sections of the junction between which the pressure loss under consideration occurs [10]. Therefore, two loss coefficients are defined to characterize a junction loss: one for straight flow (with the index st) and one for side flow (with the index s). In any case, the velocity V_c is the one in the combined flow (see Figure 2).

Based on the idea of Weitbrecht et al. [11], the following relation is used to determine the loss coefficient at the junction:

$$k = \frac{\Delta p_{i-j} - \Delta p_{f,i}}{\rho V_c^2/2}, \tag{2}$$

where Δp_{i-j} represents the pressure loss from CFD simulation and $\Delta p_{f,i}$ is the pressure loss which would occur due to friction only because of the flow from inlet to outlet of the model. It is calculated by standard pressure drop relations. According to Equation 2, equations can be written to represent all the loss coefficients with reference to Figure 2:

$$k_{\mathrm{div,st}} = \frac{\Delta p_{c-\mathrm{st}} - \left(\Delta p_{f,c} + \Delta p_{f,\mathrm{st}}\right)}{\rho V_c^2/2} \tag{3}$$

$$k_{\mathrm{div},s} = \frac{\Delta p_{c-s} - \left(\Delta p_{f,c} + \Delta p_{f,s}\right)}{\rho V_c^2/2} \tag{4}$$

$$k_{\mathrm{com,st}} = \frac{\Delta p_{\mathrm{st}-c} - \left(\Delta p_{f,\mathrm{st}} + \Delta p_{f,c}\right)}{\rho V_c^2/2} \tag{5}$$

$$k_{\mathrm{com},s} = \frac{\Delta p_{s-c} - \left(\Delta p_{f,s} + \Delta p_{f,c}\right)}{\rho V_c^2/2} \tag{6}$$

while

$$\Delta p_{c-\mathrm{st}} = p_c - p_{\mathrm{st}} \tag{7a}$$

$$\Delta p_{c-s} = p_c - p_s \tag{7b}$$

$$\Delta p_{\mathrm{st}-c} = p_{\mathrm{st}} - p_c \tag{7c}$$

$$\Delta p_{s-c} = p_s - p_c \tag{7d}$$

$$\Delta p_{f,i} = f\frac{L_i}{D_i}\frac{\rho V_i^2}{2} (i = c, s, \mathrm{st}) \tag{8}$$

where $L_c = L_{\mathrm{st}}$, as shown in Figure 2; values of $\Delta p_{c-\mathrm{st}}$, Δp_{c-s}, $\Delta p_{\mathrm{st}-c}$, and $\Delta p_{\mathrm{st}-c}$ are calculated from CFD simulations. The friction factor f can be calculated as follows:

$$f = \frac{64}{Re} \quad For\,\mathrm{Re} < 2,300, \tag{9a}$$

$$\frac{1}{\sqrt{f}} = -1.8 \log\left[\frac{6.9}{\mathrm{Re}} + \left(\frac{\epsilon/D}{3.4}\right)^{1.11}\right] \quad \mathrm{For\ Re} > 2{,}300. \tag{9b}$$

Table 1 Material and geometrical parameters of the solar collector

Description	Specification
Outside diameter of outer riser pipe (mm)	12
Inside diameter of outer riser pipe (mm)	10.4
Length of outer riser pipe (mm)	1,820
Outside diameter of inner riser pipe (mm)	6
Inside diameter of inner riser pipe (mm)	5.3
Length of inner riser pipe (mm)	1,750
Inside diameter of dividing/combining manifold pipe (mm)	22
Spacing between risers (mm)	70
Length of riser intruded inside the manifold pipe (mm)	5

CFD analysis

A 3D meshed model of a manifold connected to a riser is built in GAMBIT (Fluent Inc., Lebanon, NH, USA) as shown in Figure 3b. The mesh influences the accuracy and the simulation time of the solver. Structured meshes have a regular connectivity, which means that each point has the same number of neighbors, while unstructured meshes have irregular connectivity and each point can have a different number of neighbors. The tendency for complex configurations is to use unstructured meshes, which can be automatically generated. However, structured meshes have better accuracy compared with the same amount of unstructured meshes and need less simulation time of solver [14]. Therefore, a structured mesh (hexahedron) is used in this study.

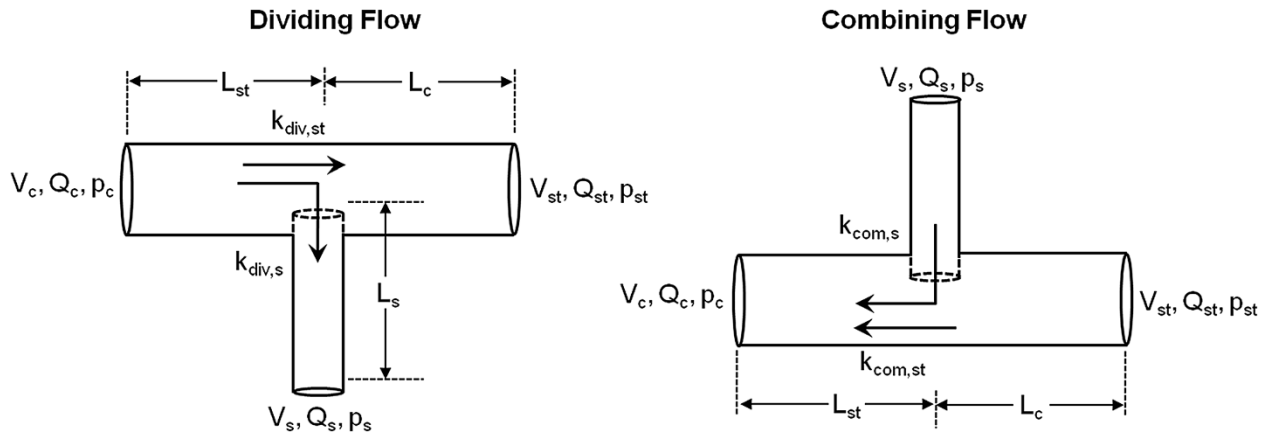

Figure 2 Loss coefficients at the dividing and combining manifold.

In order to get the structured mesh, the junction portion of the model is divided into three parts, and each part is meshed separately, as shown in Figure 3a. Initially, part 2 is meshed, then parts 1 and 3 are meshed, and at the end, the remaining straight parts of the manifold are meshed. Figure 3b shows the complete meshed model where a denser mesh is used at the junction than at other parts. The length of the manifold ($L_{st} + L_c$) is 70 mm, and the length of the riser L_s is 30 mm. The effect of mesh density was checked for a mesh density of 7.4E5 and 3.7E6 cells/m^3 which showed a negligible effect on the results. The quality of the mesh was checked based on the criteria of equiangular skew (QEAS) and equisize skew (QEVS). For more than 90% of the volume, the QEAS and QEVS are lower than 0.4, which refers to a good quality mesh.

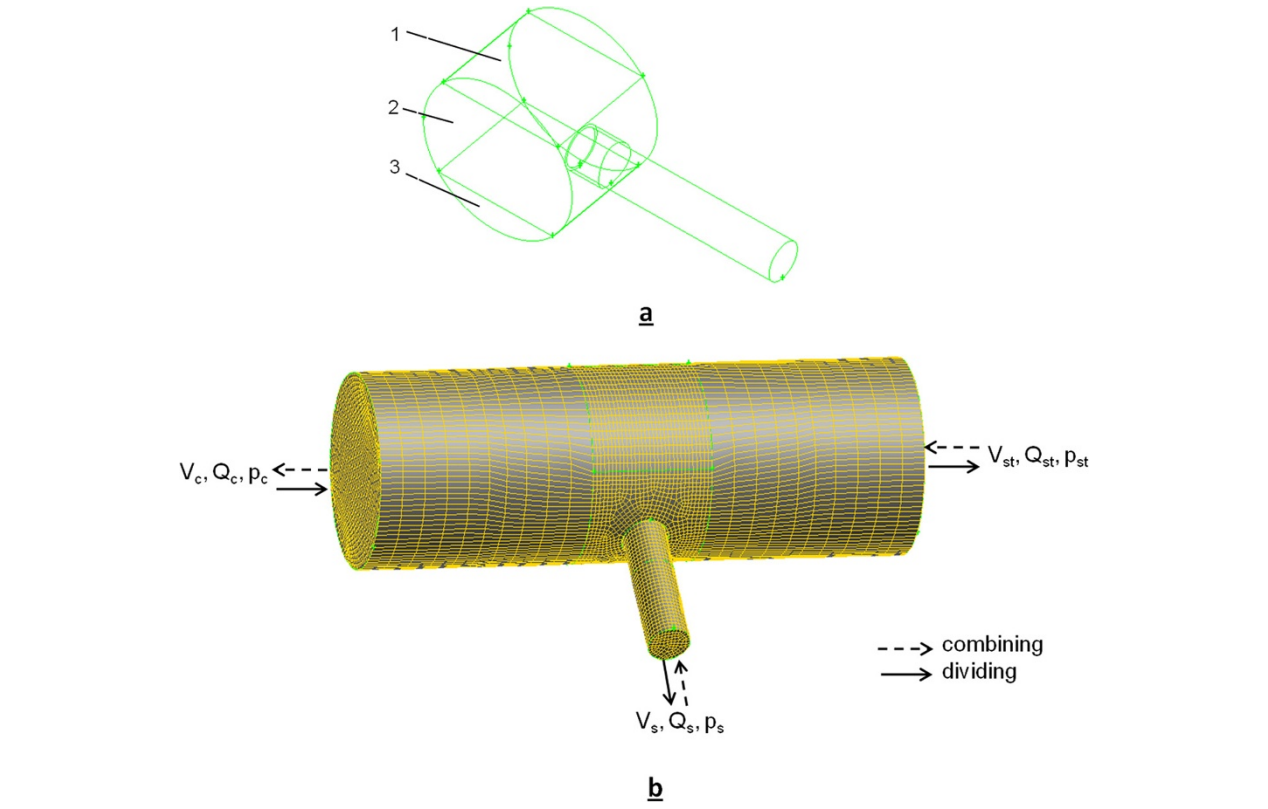

Figure 3 Schematic meshed model. (**a**) Portion of junction separated into three parts in order to have a regular mesh. (**b**) Meshed model of the manifold and riser, with higher mesh density at the junction.

The CFD code used was FLUENT 6.3.2 (Fluent Inc., Lebanon, NH, USA). The meshed model in GAMBIT is exported to FLUENT. Computations based on steady flow, pressure based, and implicit formulation are performed using CFD simulations. In this study, three viscous models are selected according to the Reynolds numbers for laminar, transition, and turbulent flows:

1. Re < 2300 laminar model
2. 2,300 ≤ Re ≤ 4,000 *k*-omega standard model (transitional flow)
3. Re > 4,000 *k*-epsilon standard model (enhanced wall treatment).

The following empirical equation is used to define the turbulence intensity:

$$I = 0.16\mathrm{Re}^{-1/8}. \tag{10}$$

Fluid properties (i.e., $\rho = 992$ kg/m^3, $\mu = 0.0010912$ kg/m s) at 80°C are used. For dividing flow with one inlet and two outlets, a uniform velocity inlet boundary condition is used for the inlet, and outflow boundary condition is used for two outlets. Outflow boundary condition is better than the pressure outlet to be used here because the ratio of flow discharge can be fixed in this boundary condition. Hence, it is possible to calculate loss coefficients for a range of riser to main manifold flow ratios.

For combining flow, there are two inlets and one outlet. The velocity inlet boundary condition is used for both inlets corresponding to a certain riser to the main manifold flow ratio. The outlet boundary condition is set to pressure outlet.

For running the program, some more specific information is required. The SIMPLE algorithm is used for pressure-velocity coupling. For faster convergence, the first-order upwind method is opted for discretization of the momentum equation, which is acceptable when the flow is aligned with the grid [15]. The standard discretization scheme is selected for the pressure. Default values for all under-relaxation factors were applied. Convergence criteria selected for the continuity, momentum, and *k*-epsilon equations are less than 5×10^{-5}, 5×10^{-5}, and 1×10^{-6}, respectively.

Hence, for both dividing and combining flow, a number of simulations were performed for a range of Reynolds numbers and riser to manifold flow ratios (Q_s/Q_c) to get the total pressure drop for the straight (manifold) and side (riser) flow. Based on area weighted average, the total pressures at the inlet and outlet faces of the manifolds then are used to calculate the loss coefficients from Equations 3 to 6.

Figure 4 shows the simulation results of the junction loss coefficients for the straight flow in the dividing manifold $k_{\mathrm{div,st}}$. It can be seen that $k_{\mathrm{div,st}}$ shows a variation with Re but negligible dependency on the considered range of flow ratios $Q_{s,i}/Q_{c,i}$. A curve is drawn to represent the trend of the resultant data which are given the form of the following equation:

$$k_{\mathrm{div,st}} = -0.219\ln(\mathrm{Re}) + 2.148 \tag{11}$$

Figure 5 illustrates the variation of the junction loss coefficients for the side flow in the dividing manifold $k_{\mathrm{div},s}$, where it can be seen that $k_{\mathrm{div},s}$ varies both with Re and ratio $Q_{s,i}/Q_{c,i}$. In order to develop an equation for $k_{\mathrm{div},s}$ with respect to Re and $Q_{s,i}/Q_{c,i}$, a procedure is

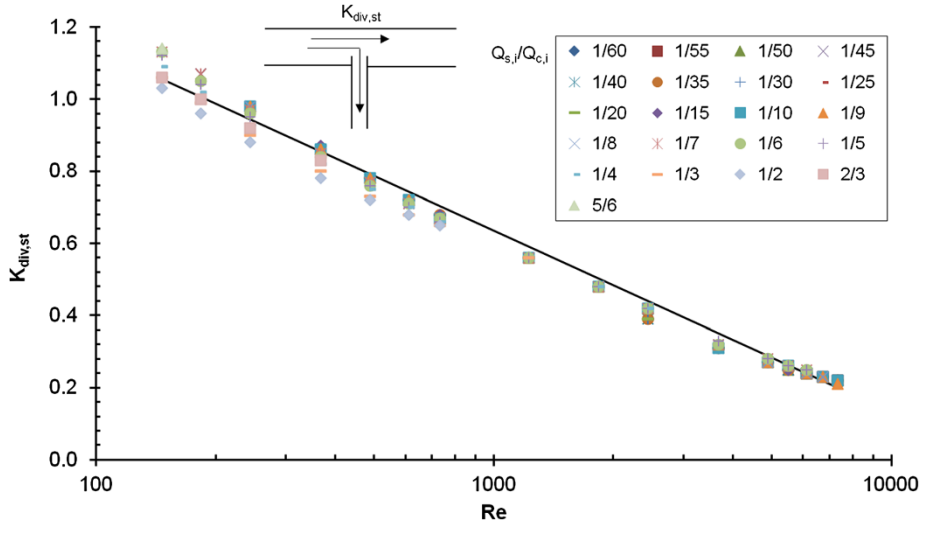

Figure 4 Variation of $k_{\mathrm{div,st}}$ with Re and $Q_{s,i}/Q_{c,i}$ and the estimated trend line.

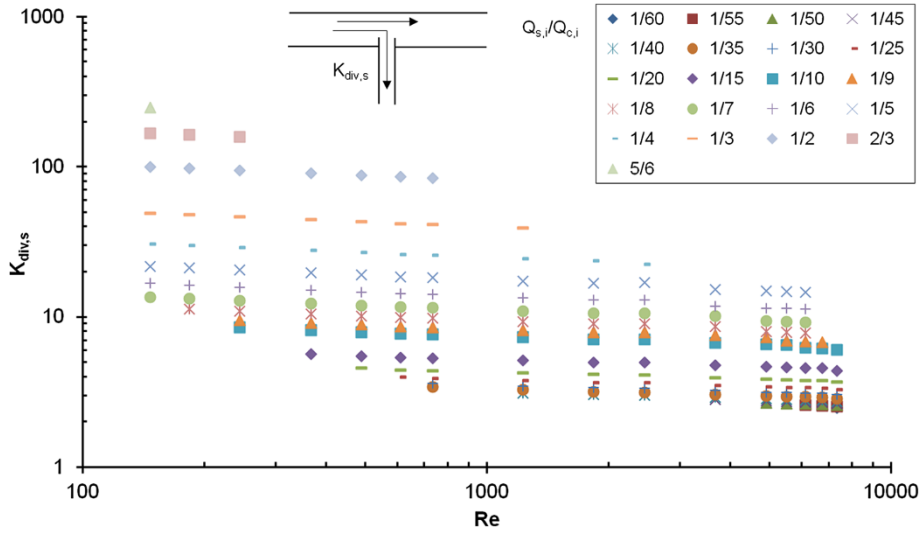

Figure 5 Variation of $k_{div,s}$ with Re and $Q_{s,i}/Q_{c,i}$.

adopted, where in the first step, each data series of $k_{div,s}$ corresponding to $Q_{s,i}/Q_{c,i}$ is fitted in a logarithmic expression in the following form:

$$k_{div,s} = a\ln(\mathrm{Re}) + b, \tag{12}$$

In the second step, coefficients a and b are plotted against the flow ratio $Q_{s,i}/Q_{c,i}$ as shown in Figure 6, which are expressed in the form of following polynomial equations to fit the trend:

$$a = -34.57\left(\frac{Q_{s,i}}{Q_{c,i}}\right) - 1.921\left(\frac{Q_{s,i}}{Q_{c,i}}\right) - 0.12, \tag{13}$$

$$b = 494\left(\frac{Q_{s,i}}{Q_{c,i}}\right)^2 + 40.71\left(\frac{Q_{s,i}}{Q_{c,i}}\right) + 3.08. \tag{14}$$

The combination of Equations 12, 13, and 14 leads to the following equation:

$$k_{div,s} = \left[-34.57\left(\frac{Q_{s,i}}{Q_{c,i}}\right)^2 - 1.921\left(\frac{Q_{s,i}}{Q_{c,i}}\right) - 0.12\right]\ln(\mathrm{Re}) + \left[494\left(\frac{Q_{s,i}}{Q_{c,i}}\right)^2 + 40.71\left(\frac{Q_{s,i}}{Q_{c,i}}\right)^2 + 3.08\right]. \tag{15}$$

Figures 7 and 8 show the junction loss coefficients for the straight and side flow in the combining manifold ($k_{com,st}$ and $k_{com,s}$). Like $k_{div,s}$, the loss coefficients for combining flow ($k_{com,st}$, $k_{com,s}$) also show variation both with Re and $Q_{s,i}/Q_{c,i}$. Notably, the values of $k_{com,s}$ increase significantly with decreasing Reynolds numbers and increasing $Q_{s,i}/Q_{c,i}$. Actually, $k_{com,s}$ becomes negative at high Re and low Q_s/Q_c,

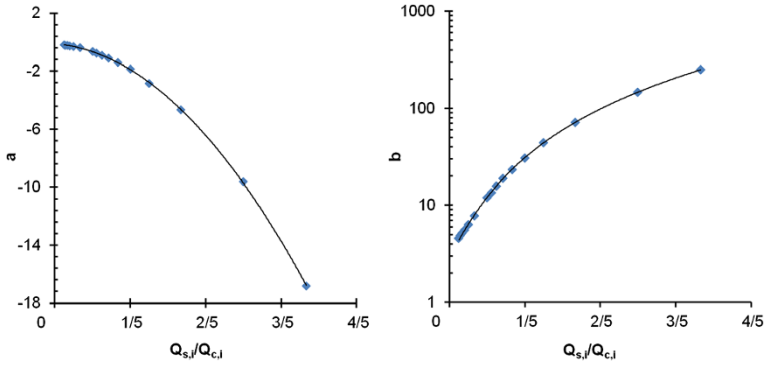

Figure 6 Coefficients a and b versus flow ratio $Q_{s,i}/Q_{c,i}$ and the fitting line.

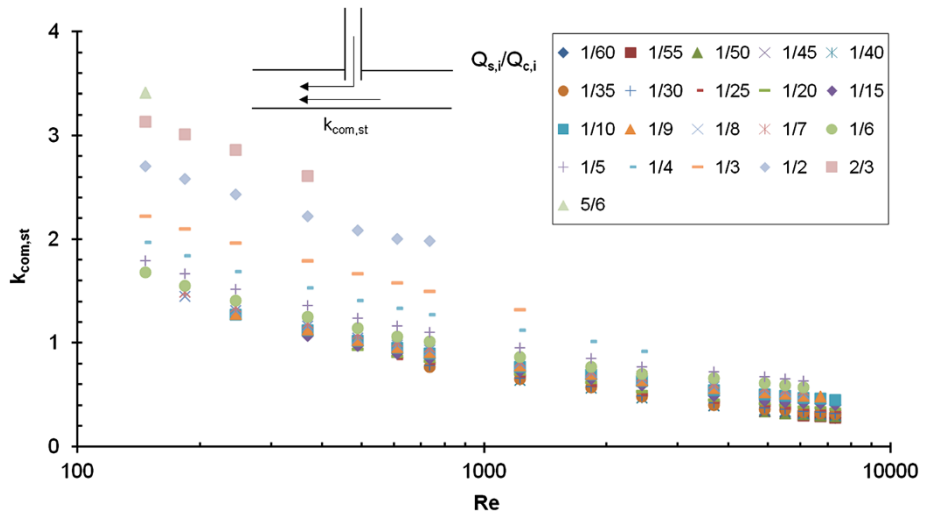

Figure 7 Variation of $k_{com,st}$ with Re and $Q_{s,i}/Q_{c,i}$.

which means there is a pressure increase in the riser at the combining junction. It is because of the fact that the velocity of the fluid in the combining manifold is much higher than the velocity of the fluid coming from the riser, and this may result in negative values of loss coefficients (also stated in the work of Idelchik [9]). By following the same method as before, the following equations are developed for $k_{com,st}$ and $k_{com,sh}$ to fit the data trend:

$$k_{\mathrm{com,st}} = 8.919\left(\frac{Q_{s,i}}{Q_{c,i}}\right)^{0.165} \cdot \mathrm{Re}^{\left[0.169\left(\frac{Q_{s,i}}{Q_{c,i}}\right)-0.306\right]}, \quad (16)$$

$$k_{\mathrm{com},s} = \left[-88.64\left(\frac{Q_{s,i}}{Q_{c,i}}\right)^{2}+1.954\left(\frac{Q_{s,i}}{Q_{c,i}}\right)-0.086\right]\ln(\mathrm{Re}) + \left[908.8\left(\frac{Q_{s,i}}{Q_{c,i}}\right)^{2}+13.381\left(\frac{Q_{s,i}}{Q_{c,i}}\right)-0.752\right]. \quad (17)$$

The maximum mean deviation of the loss coefficients between the developed equations and the values from simulation is ±6%.

Formulation of the theoretical model

Now after estimating the junction loss coefficients for the prescribed range of turbulent to laminar flow, the flow distribution through the collector consisting of 60 parallel passages can be determined theoretically by solving it as a piping network, connected either in U- or Z-configuration.

U-configuration

Figure 9 illustrates the flow network in the form of junction and frictional resistances through a parallel piping connected in U-configuration. The actual riser consisting of concentric piping is represented by a circular pipe

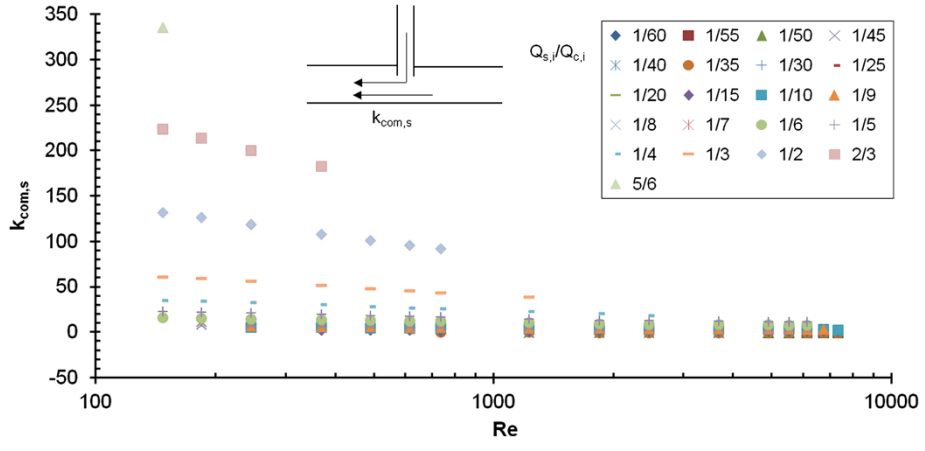

Figure 8 Variation of $k_{com,s}$ with Re and $Q_{s,i}/Q_{c,i}$.

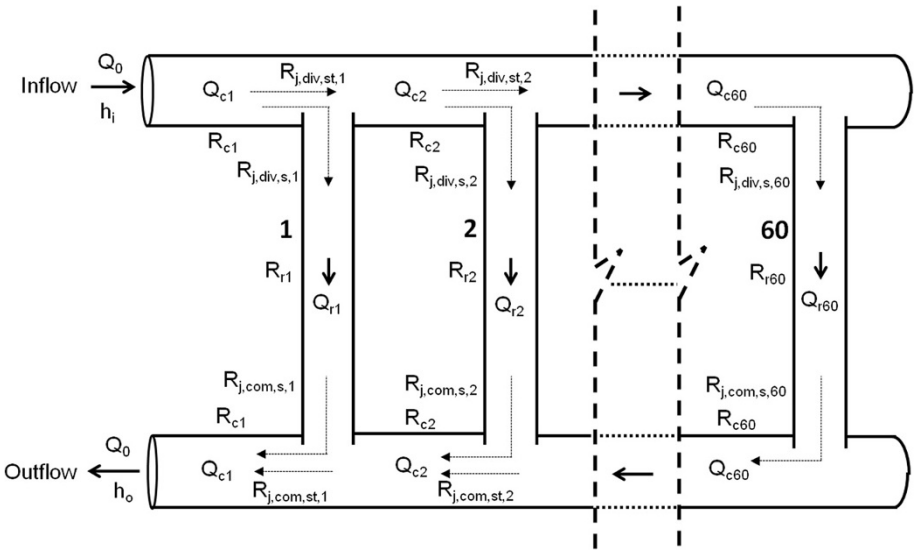

Figure 9 Schematic illustration of the flow scheme and resistances in a U-type configuration.

having equivalent resistance R_r. For each flow route through every riser from inlet to outlet, an energy equation can be written by taking into account the frictional resistance of the straight sections and the junction resistances at the branches.

For instance, it can be seen from Figure 9 that the fluid flow path through riser 1 encounters two frictional resistances through straight sections in the dividing and combining manifolds (R_{c1} and R_{c2}), two junction resistances for the side flow ($R_{j,\mathrm{div},s,1}$ and $R_{j,\mathrm{com},s,1}$), and one frictional resistances through straight section in the riser 1 R_{r1}. Thus, the overall head loss and flow through riser 1 are expressed as follows:

$$h_i - h_o = \left(2R_{c1} + R_{j,\,\mathrm{div},s,1} + R_{j,\mathrm{com},s,1}\right) {Q_{c1}}^2 + R_{r1} {Q^{r1}}_{r1}{}^2, \tag{19}$$

$$Q_{r1} = \sqrt{\frac{(h_i - h_o) - \left(2R_{c1} + R_{j,\mathrm{div},s,1} + R_{j,\mathrm{com},s,1}\right) Q_{c1}^2}{R_{r1}}}. \tag{20}$$

Similarly, in general, the flow rate through any other nth riser Q_{rn} (where, $n = 2, 3\ldots60$) can be written as follows:

$$Q_{rn} = \sqrt{\frac{(h_i - h_o) - \sum_{i=1}^{n-1}\left[\left(2R_{ci} + R_{j,\mathrm{div},\mathrm{st},i} + R_{j,\mathrm{com},\mathrm{st},i}\right) Q_{ci}^2\right] - \left(2R_{cn} + R_{j,\mathrm{div},s,n} + R_{j,\mathrm{com},s,n}\right) Q_{cn}^2}{R_{rn}}}, \tag{21}$$

where frictional and junction resistances are as follows:

$$R_{c/r} = \frac{f_{c/r} \cdot l_{c/r}}{2g d_{c/r} A_{c/r}^2}, \tag{22}$$

$$R_{j,\mathrm{div/com},s/\mathrm{st}} = \frac{k_{\mathrm{div/com},s/\mathrm{st}}}{2gA_{c/r}^2}. \tag{23}$$

The indices in Equations 22 and 23 such as $R_{c/r}$ indicate the alternative use of the equation for manifold c or riser r. The friction factors f for a circular duct (flow in the first part of the risers) is defined by Equation 9, and for annulus flow in the coaxial piping (flow in the second part - back flow - of the risers), f is given as follows:

$$f = \frac{96}{\mathrm{Re}}. \tag{24}$$

The flow at each non-branch section of the dividing or combining manifold is expressed as follows:

$$Q_{c1} = Q_o, \tag{25a}$$

$$Q_{c(i+1)} = Q_{ci} - Q_{ri}\,(i = 1, 2, \ldots, 59), \tag{25b}$$

$$Q_{c60} = Q_{r60}. \tag{25c}$$

A program is developed to solve Equations 20 to 25 in an iterative manner. For the solution of the model equations, the essential parameters such as the junction loss coefficients in Equation 23 are given by Equations 11, 15, 16, and 17 using the local Reynolds number Re and flow ratio Q_s/Q_c.

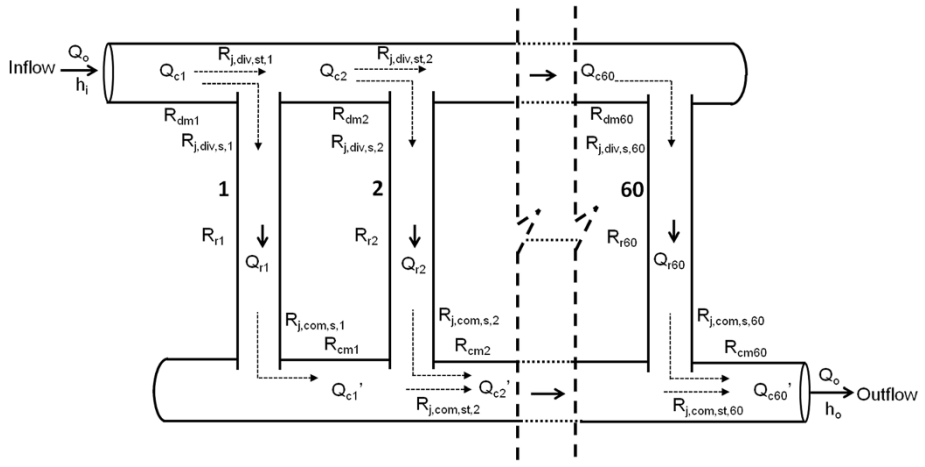

Figure 10 Schematic illustration of the flow scheme and resistances in a Z-type configuration.

Z-configuration

Figure 10 illustrates the flow network in the form of junction and frictional resistances through a parallel piping connected in Z-configuration.

For instance, it can be seen from Figure 10 that the fluid flow path from inlet to outlet through riser 1 encounters frictional resistances in dividing manifold R_{dm1}, riser R_{r1}, and combining manifolds (R_{cm1}, R_{cm2},. . ., R_{cm60}) and resistances due to junctions in dividing and combining manifolds ($R_{j,\mathrm{div},s,1}$, $R_{j,\mathrm{com},s,1}$, $R_{j,\mathrm{com,st},2}$,. . . $R_{j,\mathrm{com,st},60}$). Thus, the overall head loss and flow through riser 1 are expressed as follows:

$$h_i - h_o = \left(R_{\mathrm{dm1}} + R_{j,\mathrm{div},s,1}\right)Q_{c1}^2 + \left(R_{j,\mathrm{com},s,1} + R_{\mathrm{cm1}}\right)Q_{c1}'^2 + R_{r1}Q_{s1}^2 + \sum_{i=2}^{60}\left[\left(R_{\mathrm{cm}i} + R_{j,\mathrm{com,st},i}\right)Q_{c1}'^2\right], \quad (26)$$

The flow at each non-branch section of the dividing or combining manifold is expressed as follows:

$$Q_{c1} = Q_{c60}{}' = Q_o, \quad (29a)$$

$$Q_{c(i=1)} = Q_{ci} - Q_{ri}\,(i = 1, 2\ldots, 59), \quad (29b)$$

$$Q_{c(i+1)}{}' = Q_{ci}{}' - Q_{ri}\,(i = 1, 2\ldots, 59). \quad (29c)$$

As for the U-configuration, a program is developed to solve Equations 27 to 29 in an iterative manner for Z-configuration, by employing the same correlations for the junction loss coefficients.

Model validation

The validity of the proposed CFD based model is checked by comparing the model results with the experimentally obtained flow distribution for the same collector by Glembin et al. [2]. Their procedure was based on temperature measurements at the inlet and exit of each collector tube and using the correlation between the mass flow rate and the temperature change of the

$$Q_{r1} = \sqrt{\frac{(h_i - h_o) - \left(R_{dm1} + R_{j,div,s,1}\right)Q_{c1}^2 - \left(R_{j,com,s,1} + R_{cm1}\right)Q_{c1}'^2 - \left(\sum_{i=2}^{60}\left[\left(R_{cmi} + R_{j,st,com,i}\right)Q_{ci}'^2\right]\right)}{R_{s1}}}. \quad (27)$$

In general, the flow rate through any other nth riser Q_{rn} (where $n = 2, 3\ldots, 60$) can be written as follows:

$$Q_{rn} = \sqrt{\frac{(h_i - h_o) - \sum_{i=1}^{n}\left(R_{\mathrm{dm}i}Q_{ci}^2\right) - \sum_{i=1}^{n-1}\left(R_{j,\mathrm{div,st},i}Q_{ci}^2\right) - R_{j,\mathrm{div},s,n}Q_{sn}^2 - \sum_{i=n}^{60}\left(R_{\mathrm{cm},i}Qr_{ci}^2\right) - \sum_{i=n}^{60}\left(R_{j,\mathrm{com,st},i}Qr_{ci}^2\right) - R_{j,\mathrm{com},s,n}Qr_{cn}^2}{R_{rn}}}. \quad (28)$$

fluid while flowing through each collector tube. The experiments were performed for a mass flow range of 200 to 500 kg/h (or $M = 78$ to 31 kg/m^2 h) and an inlet temperature T_{fi} range of 20°C to 80°C. A flow ratio ϵ was calculated, which is used here to compare our modeling results. The flow ratio ϵ is defined as the actual flow Q_{ri} through a riser i to the averaged flow Q_{av} through all risers. It is given as follows:

$$\epsilon = \frac{Q_{ri}}{Q_{\text{av}}} = \frac{Q_{ri}}{Q_o/60}. \tag{30}$$

However, these data have not been reported for each experiment but only the average distribution over all experiments.

To account for the temperature effects on fluid properties such as viscosity and density of the fluid, the arithmetic mean of the measured inlet-outlet temperate for each tube (also taken from the work of Glembin et al. [2]) is used to calculate the viscosity and density of the fluid in the respective risers and outlet manifold sections. The estimated junction loss coefficients have shown negligible variation with the temperature.

The details of all the chosen flow rates and inlet temperatures (in the described ranges) of the conducted experiments are not reported in the article of Glembin et al. [2]; therefore, a total of four extreme points of operation corresponding to a flow rate of 78 and 31 kg/m^2 h and inlet temperatures of 20°C and 80°C are selected to compute the flow distribution numerically.

Figure 11 shows the calculated flow distributions for the considered range along with the net averaged flow distributions from the experiment. It can be seen that for a certain inlet temperature ($T_{fi} = 80$°C or 20°C), the overall flow rate has some influence on the flow distribution, i.e., nonuniformity decreases with decreasing flow rate (as shown by Fan et al. [4] and Weitbrecht et al. [11]). However, on the other hand, for a certain mass flow rate ($M = 78$ or 31 kg/m^2 h), the change of inlet temperature from 80 to 20°C shows a larger impact on the calculated flow distribution. With decreasing temperature, viscosity increases and hence the Reynolds number decreases, which results in higher pressure drop for laminar flow through the risers, and this leads to more uniform flow distribution. This variation of Reynolds number in each riser for the above four cases is also shown in Figure 12.

From the simulation, it can be concluded that the use of an average flow distribution as done by Glembin et al. [2] is not really sensible. However, as the averaged experimental curve falls well in between the simulated flow distribution, a reasonable agreement can be stated. Deviations mainly stem from the Reynolds number dependency of the flow distribution. Other reasons for disagreement are the strong sensitivity of the junction loss coefficients at very low Reynolds numbers, geometrical simplification of the actual branch region for the CFD simulation (see Figures 1b and 2), the complexity of the fluid flow in the real conditions, the assumption of fully developed flow in the whole collector, the unknown error margin of the measurements, and the details regarding the tested range of inlet fluid temperatures (between 20°C and 80°C) for the derived experimental flow distribution curve.

Results and discussion

We know that the geometry of the manifold (i.e., simplification of the actual branch region involving flexible

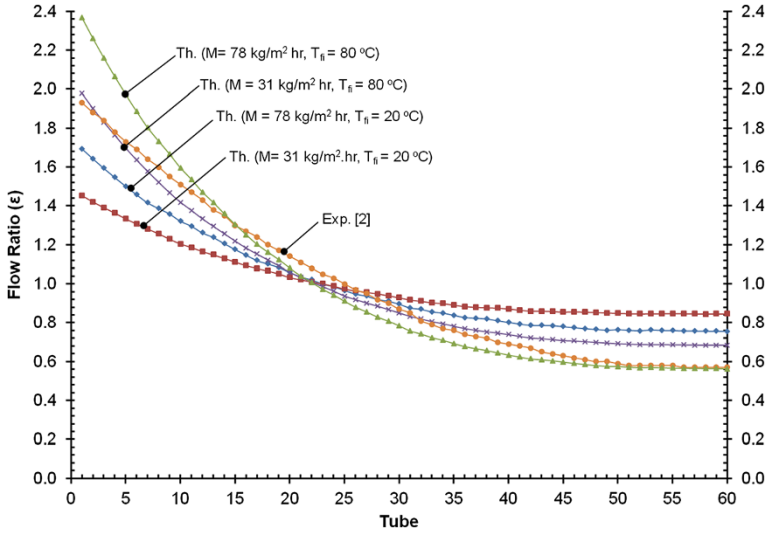

Figure 11 Measured and calculated non-isothermal flow distribution for U-configuration.

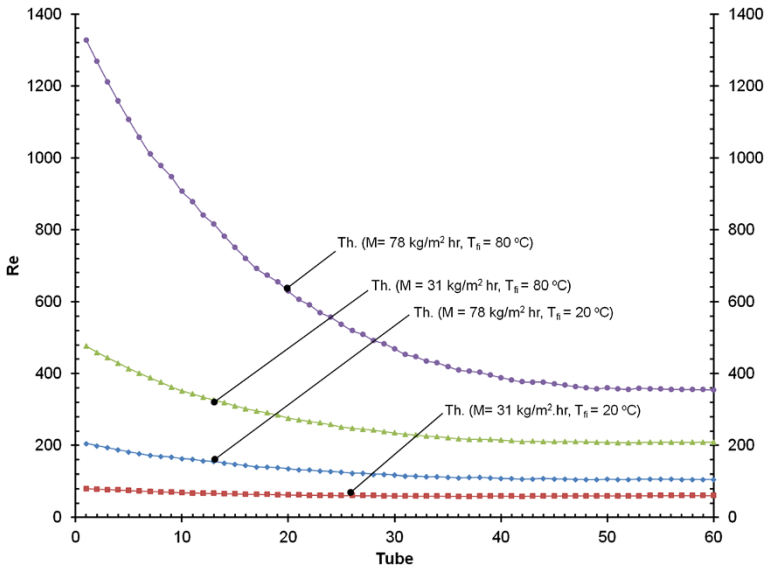

Figure 12 Variation of the Reynolds number in the inner circular pipe of each riser.

corrugated piping, chosen lengths of riser, and manifold as shown in Figures 1, 2, and 3) and boundary conditions which were used for the FLUENT simulation approximates but may not describe the real conditions which prevail inside the manifold at each branch region due to the influence of adjacent branches and the manner in which the flow is changing (decreasing or increasing) in the manifolds. The worse outcome of these assumptions and simplifications could be that estimated values of loss coefficients are too small or too large (if still assuming, the trend of k's as function of Re and flow ratio Q_s/Q_c remains the same as shown in Figures 4, 5, 6, 7, and 8). Therefore, a sensitivity analysis is performed, where the loss coefficients at the junctions are varied over a certain range to see their effect on the estimated flow distribution. For that purpose, isothermal flow distribution for $M = 78$ kg/m^2 h based on junction loss coefficients ($k_{\mathrm{div,st}}$, $k_{\mathrm{div},s}$, $k_{\mathrm{com,st}}$, and $k_{\mathrm{com},s}$) given by Equations 11, 15, 16, and 17 is used as the reference, and the influence of increasing or decreasing the loss coefficients for straight ($k_{\mathrm{div,st}}$ and $k_{\mathrm{com,st}}$) and side flow ($k_{\mathrm{div},s}$ and $k_{\mathrm{com},s}$) is examined. It is also useful to determine which loss coefficients have a critical influence on the flow distribution.

Figures 13 and 14 show the resulting flow distribution by varying the junction loss coefficients for the side flow ($k_{\mathrm{div},s}$ and $k_{\mathrm{com},s}$) and straight flow ($k_{\mathrm{div,st}}$ and $k_{\mathrm{com,st}}$) from the reference case in the range of −40% to +40%, respectively. It can be seen that side flow coefficients

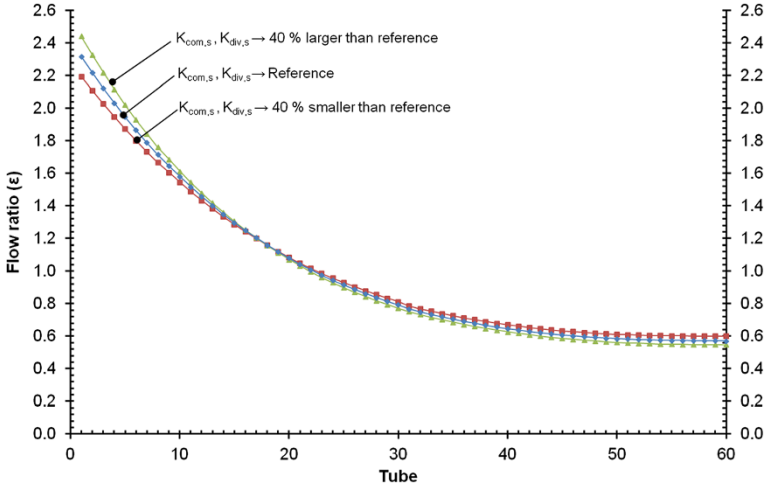

Figure 13 Isothermal flow distribution at $M = 78$ kg/m^2 h for U-configuration by varying $k_{\mathrm{div},s}$ and $k_{\mathrm{com},s}$. The distribution is in the range of −40% to 40% of the reference.

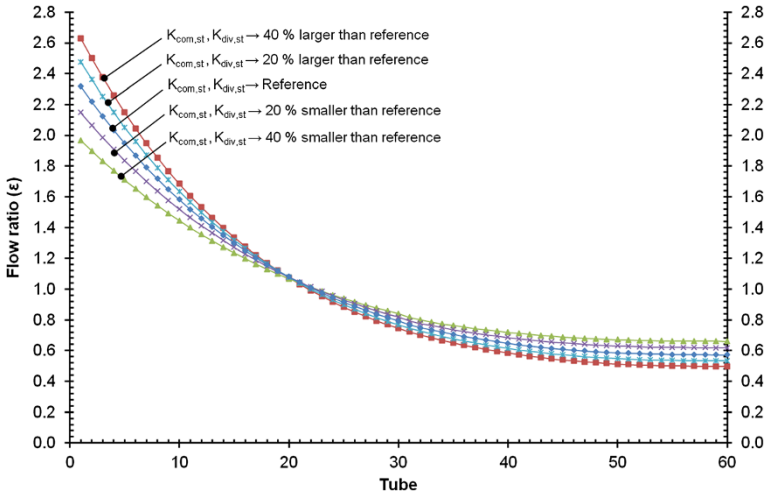

Figure 14 Isothermal flow distribution at $M = 78$ kg/m^2 h for U-configuration by varying $k_{div,st}$ and $k_{com,st}$. The distribution is in the range of −40% to 40% of the reference.

($k_{div,s}$ and $k_{com,s}$) have a marginal effect on the flow distribution by increasing or decreasing it in the range of −40% to +40% (Figure 13), while the straight flow coefficients result in a higher deviation from the reference case in the same range (Figure 14), but still, the deviation is not so drastic from the reference. This can be explained in a way that, for example, a fluid particle which is flowing through the 30th riser has to encounter 29 straight flow junction losses ($k_{div,st}$ and $k_{com,st}$) in the dividing and combining manifolds and only two side flow junction losses ($k_{div,s}$ and $k_{com,s}$) in the 30th riser (see Figure 9). It can be concluded that straight flow junction loss coefficients are more critical in finding the correct flow distribution.

The CFD-based model is now used to investigate various aspects of the flow distribution mechanism. Figure 15 illustrates the comparison of the calculated flow distribution based on the junction loss coefficients from CFD simulations at low Reynolds numbers and the available correlations for turbulent flows from Idelchik [9] and Bassett et al. [10]. It is seen in Figure 15 that the resulting flow distribution curves for Idelchik [9] and Bassett et al. [10] are almost identical but differ appreciably from the present case. The main reason for this deviation is the low values of the junction loss coefficients of the straight flow ($k_{div,st}$ and $k_{com,st}$) from the correlations of Idelchik [9] and/or Bassett et al. [10] depicted in Figure 16 for the encountered range of Reynolds number from 70 to 7,000 (corresponding to total mass flow of 78 kg/m^2 K) in the manifolds.

Figure 17 shows the flow distribution for increasing length of the riser while keeping the geometrical

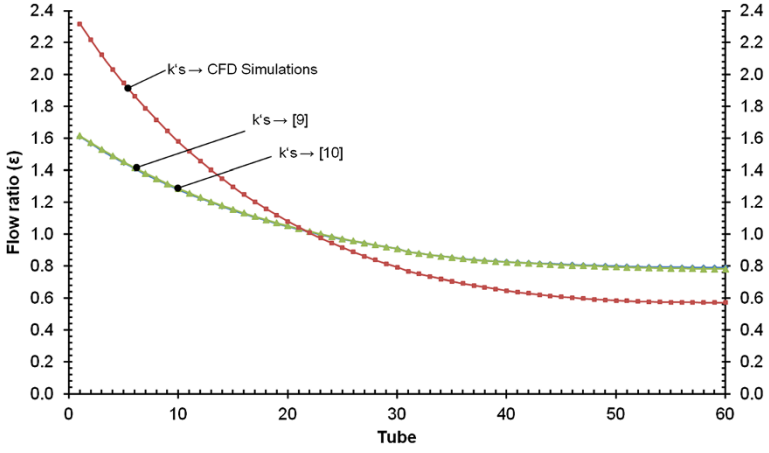

Figure 15 Comparison of isothermal flow distribution (U-configuration) for junction loss coefficients. Based on CFD simulations, Idelchik [9] and Bassett et al. [10] at $M = 78$ kg/m^2 h.

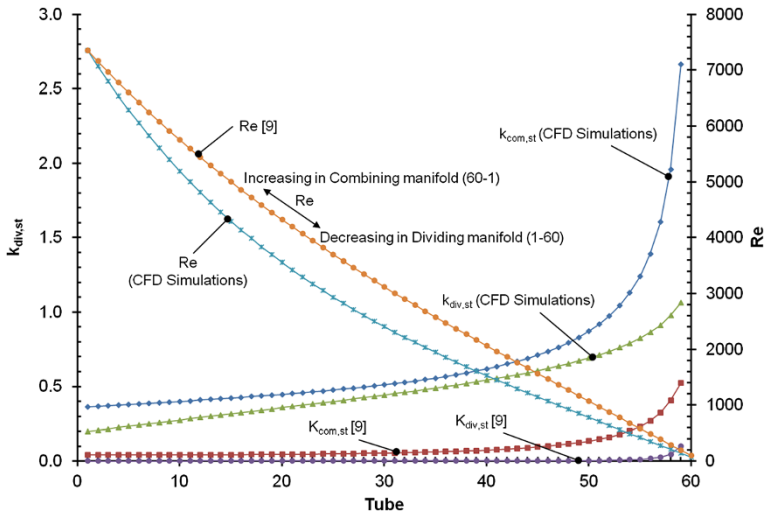

Figure 16 Variation of $k_{div/com,st}$ at each branch of dividing and combining manifold. Based on CFD simulations Idelchik [9] for U-configuration at $M = 78$ kg/m^2 h.

parameters of the manifolds the same (see Table 1). It is obvious that flow uniformity increases with increasing riser length from 1.82 to 8 m, which leads to a well-known principle regarding flow distribution in manifolds, i.e., higher pressure drop in the risers as compared with the manifolds results in more uniform flow distribution.

Finally, the flow distribution is also calculated for the Z-configuration, and comparison is made for the same collector connected in the U- and Z-configurations (Figure 18). For the Z-configuration, the flows are higher at the ends and lower in the middle tubes; they show a similar trend as predicted by McPhedran et al. [1] for 60 tubes and also in good agreement with the experimental results of Glembin et al. [16]. The Z-configuration results in more uniform flow (ϵ is near to unity). The minimum flow ratio ϵ and thus the minimum riser flow rate reached in the case of the Z-configuration (0.8) is 20% higher than for the case of the U-configuration (0.6). However, even in Z-configuration, the flow distribution is not at all uniform.

Conclusions

A CFD analysis is used to estimate the junction losses at the tee junctions of a collector manifold. A simplified model of the junction is built and simulated in FLUENT for a range of Reynolds numbers and riser-to-manifold flow ratios. The resulting junction loss coefficients have

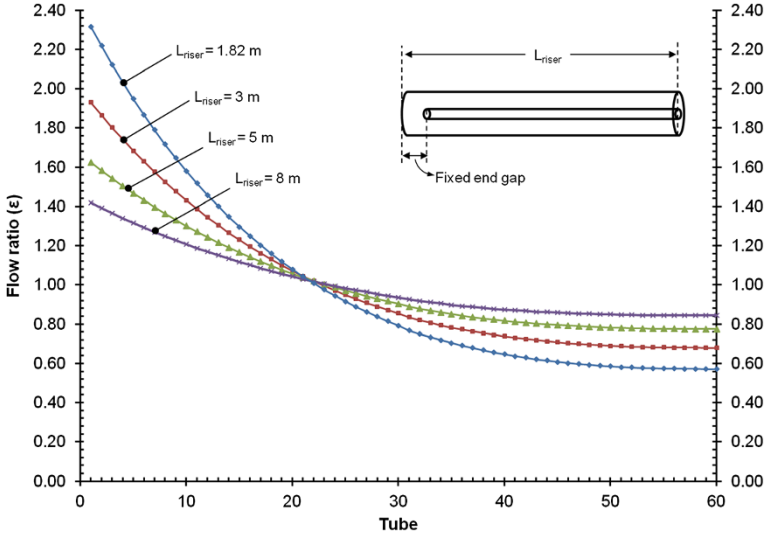

Figure 17 Isothermal flow distribution with increasing riser length for U-configuration at $M = 78$ kg/m^2 h.

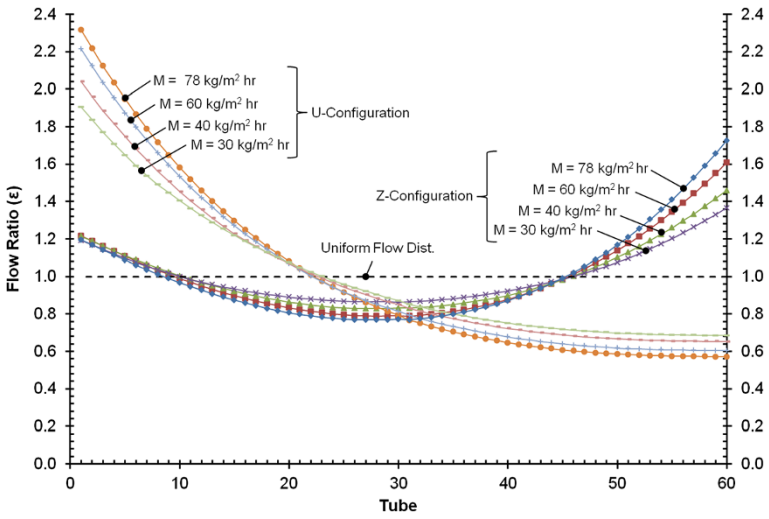

Figure 18 Isothermal flow distribution curves for U- and Z-configuration.

shown a strong dependency on the flow rate at low Reynolds numbers.

The variable loss coefficients are implemented in a theoretical model to predict the flow distribution in a coaxial vacuum tube solar collector arranged in U- and/or Z-configurations. The model is validated with the experimental results for the same collector in U-configuration. The model agrees reasonably well (but not perfectly) to the experiments. The model can be used to predict flow distribution for any number of risers in the prescribed range of Reynolds numbers. Flow uniformity decreases with increasing flow rate and temperature. Parallel flow (Z-configuration) results in more but not perfectly uniform flow than the reverse flow (U-configuration). The proposed CFD-based method can replace the expensive and time-consuming procedure of setting up experiments for estimating junction losses.

Abbreviations

Nomenclature

D: Diameter (m); F: moody friction factor (–); $h_i - h_o$: head loss (m); I: turbulence intensity; K: pressure loss coefficient (–); $k_{com,s}$: local pressure loss coefficient for combining side flow (–); $k_{com,st}$: local pressure loss coefficient for combining straight flow (–); $k_{div,s}$: local pressure loss coefficient for dividing side flow (–); $k_{div,st}$: local pressure loss coefficient for dividing straight flow (–); L: length (m); P: pressure (Pa); Δp: pressure drop (Pa); Δp_{c-s}: pressure drop between the inlet manifold and the riser in dividing flow (Pa); Δp_{c-st}: pressure drop between the inlet manifold and the straight outlet manifold in dividing flow (Pa); Δp_f: pressure drop due to friction (Pa); Δp_{fth}: theoretical calculated pressure drop due to friction (Pa); $\Delta p_{f,c}$: pressure drop in combined manifold due to friction (Pa); $\Delta p_{f,s}$: pressure drop in riser due to friction (Pa); $\Delta p_{f,st}$: pressure drop in straight manifold due to friction (Pa); Δp_{s-c}: pressure drop between the riser and the outlet manifold in combing flow (Pa); Δp_{sim}: pressure drop calculated from simulation (Pa); Δp_{st-c}: pressure drop between the straight inlet manifold and the outlet manifold in combing flow (Pa); Q: volume flow (m^3/s); Q_o: total volume flow (m^3/s); R: frictional resistance (s^2/m^5); R_c: frictional resistance for the flow through dividing or combining manifold in U-configuration (s^2/m^5); R_{dm}: frictional resistance for the flow through dividing manifold in Z-configuration (s^2/m^5); R_{cm}: frictional resistance for the flow through combining manifold in Z-configuration (s^2/m^5); $R_{j,div,s/st}$: junction resistance for the side or straight flow in dividing manifold (s^2/m^5); $R_{j,com,s/st}$: junction resistance for the side or straight flow in combining manifold (s^2/m^5); Re: Reynolds number (–); T_{fi}: Temperature of fluid at inlet (°C); V: Velocity (m/s).

Greek symbols

ϵ: Roughness (m) (Equation 9b); ϵ: flow ratio (–) (Equation 30); μ: dynamic viscosity (kg/m s); ρ: density (kg/m^3).

Subscripts

av: Averaged; *c*: combined; *cr*: combining manifold in Z-configuration; *r*: riser; *s*: side; st: straight.

Competing interests

The authors declare that they have no competing interests.

Authors' contributions

AWB developed and programmed the numerical model for calculating the flow distribution and drafted the manuscript. RB collected the data, conducted the initial study, carried out initial analysis, and participated in the design and coordination of the study. YL participated in the design of the study, constructed the model geometry for simulation, performed simulations, and developed equations to be used in the numerical model. FZ checked the whole work critically and edited and corrected the draft manuscript. All authors read and approved the manuscript.

Received: 12 July 2012 Accepted: 15 August 2012
Published: 19 September 2012

References

1. McPhedran, R.C., Mackey, D.J.M., McKenzie, D.R., Collins, R.E.: Flow distribution in parallel connected manifolds for evacuated tubular solar collectors. Aust. J. Phys. **36**, 197–219 (1983)
2. Glembin, J., Rockendorf, G., Scheuren, J.: Internal thermal coupling in direct-flow coaxial vacuum tube collectors. Solar Energy **84**, 1137–1146 (2010)
3. Viller, N.M., López, J.M.C., Munoz, F.D.: Numerical 3-D heat flux simulations on flat plate solar collectors. Solar Energy **93**, 1086–1092 (2009)
4. Fan, J., Shah, L.J., Furbo, S.: Flow distribution in a solar collector panel with horizontally inclined absorber strips. Solar Energy **81**, 1501–1511 (2007)
5. Wang, X.A., Yu, P.: Isothermal flow distribution in header systems. Solar Energy **7**, 159–169 (1989)
6. Wang, X.A., Wu, L.G.: Analysis and performance of flat-plate solar collector arrays. Solar Energy **45**, 71–78 (1990)
7. Jones, G.F., Lior, N.: Flow distribution in manifold solar collectors with negligible buoyancy effects. Solar Energy **52**, 289–300 (1994)
8. Fan, J., Furbo, S.: Buoyancy effects on thermal behaviour of a flat-plate solar collector. J Solar Energy Eng **130**(1–12), 021010 (2008)

9. Idelchik, I.E.: Handbook of Hydraulic Resistance, 2nd edn. Springer, Washington (1986)
10. Bassett, M.D., Winterbone, D.E., Pearson, R.J.: Calculation of steady flow pressure loss coefficients for pipe junctions. Proceedings of the institution of mechanical engineers, part C. J. Mech. Eng. Sci. **215**, 861–881 (2001)
11. Weitbrecht, V., Lehmann, D., Richter, A.: Flow distribution in solar collectors with laminar flow conditions. Solar Energy **73**, 433–441 (2002)
12. Buchholz, R.: Hydraulische Untersuchung einer Vakuumröhren Kollektoranlage in Hinsicht auf einen möglichen partiellen Stilstand und damit verbundenen leistungseinbußen. Institut für Energietechnik, Technische Universität, Berlin (2005)
13. Tyfocor, L.S.: Technische Information. P. TYFOROP CHEMIE GmbH, Hamburg (1999). http://www.tyfo.de
14. Filipiak, M.: Mesh Generation. Edinburgh parallel computing centre, the University of Edinburgh, Edinburgh (1996)
15. Fluent Inc: Fluent 6.3 UDF Manual. Fluent Inc, Lebanon (2006)
16. Glembin, J., Eggert, D., Rockendorf, G., Scheuren, J.: Evaporation in solar thermal collectors during operation - reasons and effects of partial stagnation. J Solar Energy Eng **133**(1–9), 041003 (2011)

doi:10.1186/2251-6832-3-24
Cite this article as: Badar *et al.*: CFD based analysis of flow distribution in a coaxial vacuum tube solar collector with laminar flow conditions. *International Journal of Energy and Environmental Engineering* 2012 **3**:24.